Structure Evolution and Thermoelectric Properties of Carbonized Polydopamine Thin Films

Haoqi Li,[†] Yaroslav V. Aulin,[‡] Laszlo Frazer,[‡] Eric Borguet,[‡] Rohit Kakodkar,[§] Joseph Feser,[§] Yan Chen,[∥] Ke An,[∥] Dmitriy A. Dikin,[†] and Fei Ren*,[†]

[†]Department of Mechanical Engineering and [‡]Department of Chemistry, Temple University, Philadelphia, Pennsylvania 19122, United States

[§]Department of Mechanical Engineering, University of Delaware, Newark, Delaware 19716, United States

[∥]Chemical and Engineering Materials Division, Oak Ridge National Laboratory, Oak Ridge, Tennessee 37831, United States

Ⓢ Supporting Information

ABSTRACT: Carbonization of nature-inspired polydopamine can yield thin films with high electrical conductivity. Understanding of the structure of carbonized PDA (cPDA) is therefore highly desired. In this study, neutron diffraction, Raman spectroscopy, and other techniques indicate that cPDA samples are mainly amorphous with some short-range ordering and graphite-like structure that emerges with increasing heat treatment temperature. The electrical conductivity and the Seebeck coefficient show different trends with heat treatment temperature, while the thermal conductivity remains insensitive. The largest room-temperature ZT of 2×10^{-4} was obtained on samples heat-treated at 800 °C, which is higher than that of reduced graphene oxide.
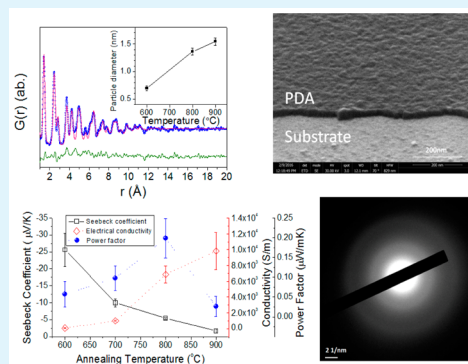
Polydopamine (PDA) is a nature-inspired material obtained through polymerization of biomolecule dopamine (Figure 1a), which can be synthesized under mild aqueous conditions simulating marine environments. PDA exhibits strong affinity to a wide range of surfaces[1] due to the existence of multiple functional groups, which can be attached to organic and inorganic materials.[2] Therefore, PDA has been proposed to serve as a universal platform for various surface modifications.

Despite this wide range of applications, the structure of PDA is still under debate. The prevailing opinions believe[3−5] that PDA is not a polymer but stacked oligomers. Meng and Kaxiras[3] proposed that the oligomers form stacked layers or helical structures through C−C bonding. Hong et al.[4] believed that covalent bonding contributed to the formation of oligomers while noncovalent bonding such as hydrogen bonding and π−π interaction were the primary mechanisms for interlayer stacking. Using experimental and simulation techniques, Liebscher et al.[5] showed the oligomer interactions were primarily charge transfer with possible hydrogen bonding. Furthermore, the authors proposed that the oligomers were likely linear, yielding structures similar to that shown in Figure 1b.[5] In contrast, Dreyer and co-workers[6] proposed a different model where PDA does not possess covalent bonding but consists of individual monomers held together by noncovalent bonding such as charge transfer, π−π interaction, and hydrogen bonding.

PDA can be carbonized by pyrolysis, and carbonized PDA (cPDA) exhibits high electrical conductivity similar to or even greater than reduced graphene oxides.[7,8] For example, Li et al.[7] reported high electrical conductivity in cPDA, up to 1.2×10^5 S/m after heat treatment at 1000 °C in Ar/H₂. Kong and co-workers[8] also found the electrical conductivity of cPDA film was as high as 2.6×10^5 S/m. It is speculated that cPDA might have a structure similar to that shown in Figure 1c,[9] which could be considered as nitrogen-doped graphite.

Using transmission electron microscopy, Kong et al. observed layered carbon structures in the cPDA film coated on SnO₂ particles, and proposed that cPDA could be regarded as multilayer graphene.[8] Additional evidence showing the layered structure of cPDA was obtained in a TEM study performed by Yu and co-workers,[10] where an interlayer d-spacing of 0.34 nm was observed. However, X-ray diffraction on cPDA materials showed inconsistent results. Kong et al.[8] and Ryu et al.[11] both found a peak around $2\theta = 22°$, which corresponds to a d-spacing of 0.44 nm. In contrast, an earlier study on PDA by Ryu and co-workers[12] showed two XRD peaks at $2\theta = 25.7°$ and $2\theta = 12.8°$, which correspond to d-spacings of 0.347 and 0.692 nm, respectively. Raman spectroscopy was also performed to study the structure of

(a)   (b)   (c)
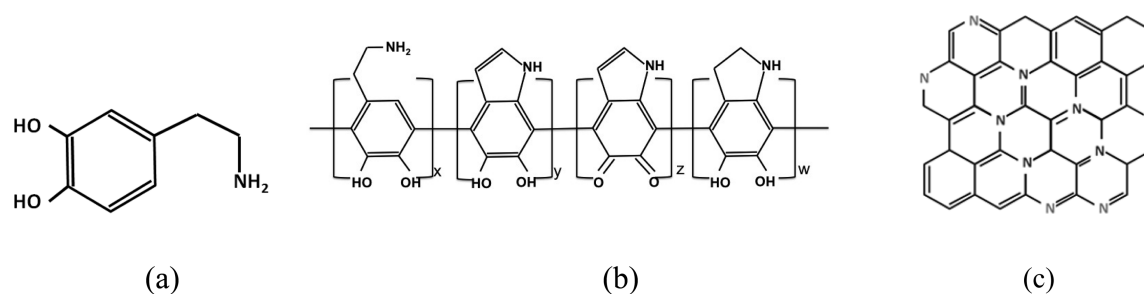
Figure 1. Schematics showing (a) the dopamine molecule, (b) a proposed PDA structure based on covalently bonded linear oligomers.[5] (c) a hypothetical structure of carbonized PDA.[9] Reproduced with permission from ref 5. Copyright 2013 American Chemical Society. Reproduced with permission from ref 9. Copyright 2012 John Wiley and Sons.
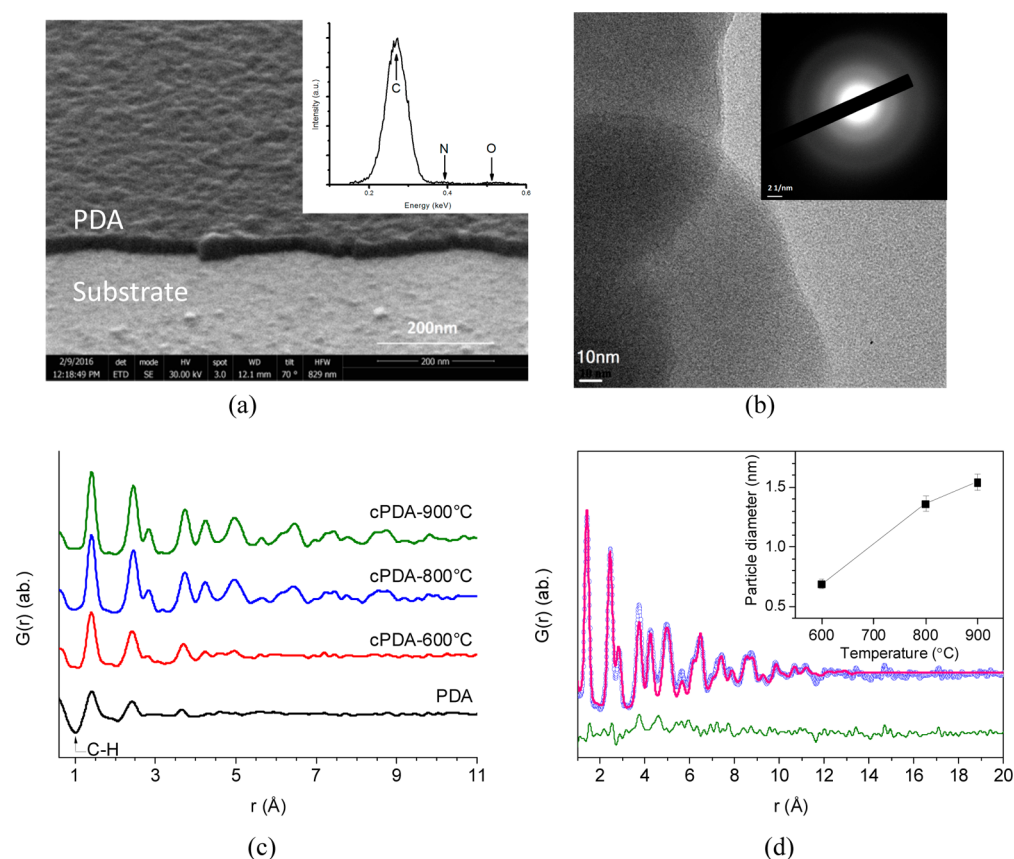

Figure 2. (a) SEM image of PDA film, inset is the energy-dispersive spectrum. (b) TEM image of carbonized PDA powder, inset is electron diffraction. (c) Neutron pair distribution functions (PDFs) of PDA and carbonized PDA powders at different temperatures and (d) fitting of PDF of cPDA-900 °C using the graphite structure. The blue dots, pink line, and green line are the observed data, fit data, and the difference, respectively. The inset shows the average particle diameters as a function of annealing temperature, which were extracted from the PDF fitting.

cPDA materials. Yu et al.[10] identified two peaks in the Raman spectrum of cPDA after being heat-treated at 800 °C: 1331 and 1578 cm^{-1}, corresponding to the D and G bands of graphitic materials.[13,14] It is worthwhile to note that the intensity ratio between the D and G bands, I_D/I_G, is greater than unity.[10] Ryu and co-workers[11] also studied the Raman spectroscopy of cPDA pyrolyzed at 1050 °C and found $I_D/I_G = 0.86$, which is lower than that obtained from PDA ($I_D/I_G = 0.94$).

In this work, structural evolution of PDA as a function of the level of carbonization was studied using electron microscopy, Raman spectroscopy, and neutron scattering. In addition, room-temperature Seebeck coefficient, electrical conductivity, and thermal conductivity of PDA thin films carbonized at different temperatures were examined.

The as-coated PDA films possessed a brownish color, which gradually changed to black as the heat treatment temperature increased. SEM examination showed the PDA films, before and after heat treatment, were continuous across large distance (>100 μm) without surface cracks or porosity (Figure 2a). AFM measurements at multiple locations indicated that the thicknesses of the film is uniform (Figure S3) with surface roughness less than 1.2 nm (Table S1).

Figure 2a shows an SEM image of cPDA film after heat treatment at 800 °C in Ar. The inset of Figure 2a is an energy-dispersive X-ray spectroscopic (EDS) profile showing that the cPDA film is primarily consisted of carbon with a small amount of oxygen and nitrogen (Figure 1). XRD measurements showed similar spectra for PDA and cPDA samples (Figure S5). No
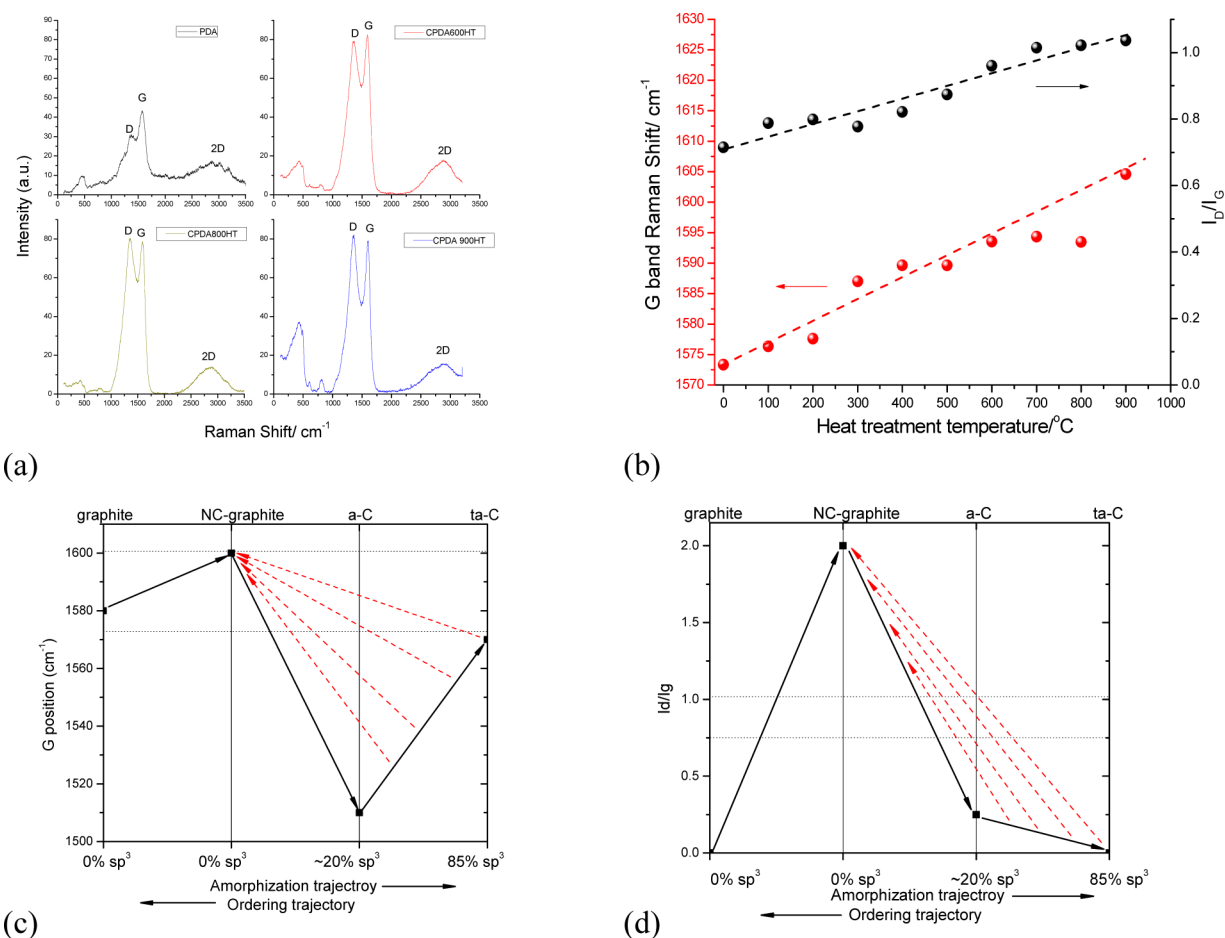
Figure 3. (a) Selected Raman spectra of PDA and cPDA samples with various heat treatment temperatures. (b) G peak position and I_D/I_G as a function of heat treatment temperature. (c) Migration of the G band position with respect to the crystallization degree[13] and (d) change of the I_D/I_G ratio as a function of the crystallization degree.[13] The solid lines in c and d indicate the paths for pure graphite, while the dash lines indicate the ordering trajectories of graphite with impurities. Reproduced with permission from ref 13. Copyright 2004 The Royal Society.

well-defined peaks could be identified except a broad peak around 21°, which corresponds to 0.42 nm spacing and is similar to those reported by Kong[8] and Ryu.[11] TEM analysis of the PDA and cPDA powder samples revealed mainly amorphous structures. Figure 2b shows a TEM image of cPDA particles heat treated at 800 °C, where no distinct crystalline or layered features could be identified. Selected area electron diffraction (SAED) showed two diffused rings at approximately 5 nm⁻¹ and 8.7 nm⁻¹ (inset of Figure 2b), corresponding to some ordering with a spacing of 0.2 and 0.12 nm, respectively. The spacing of 0.12 nm is likely related to acetylene-type triple bonds and the nature of the 0.2 nm ordering is unclear.

Neutron total scattering experiments were performed on the PDA powders and the cPDA powders heat-treated at 600 °C (cPDA-600), 800 °C (cPDA-800), and 900 °C (cPDA-900). The neutron pair distribution functions (PDF) that characterize the local structures were measured and fitted with the graphite structure model (Figures 2c, d). The peaks at small r (interatomic spacing) region confirm the short-range correlations of the atoms. The local structure is consistent for the annealed cPDA powders of different temperatures, whereas it is different from that of the PDA powders (Figure 2c). The comparison shows the structure evolutions from annealing at high temperatures. A feature of negative peak at $r = 1.07$ Å is observed in the PDA. It is likely due to C−H, N−H, or O−H

bonds because hydrogen possesses a negative neutron scattering length and the correlation length agrees with the average bond lengths. This negative peak feature is still observable in cPDA-600 however completely diminished in cPDA-800 and cPDA-900 as a result of fully removal of the hydrogen during carbonization.

The high temperature annealing promotes the local ordering and particle growth. PDA may be considered as a doped amorphous carbon (a-C) that consists of a mixture of sp3 and sp2 bonds. When subject to thermal annealing, a-C has the tendency to convert to either graphite (under low pressure) or diamond (under high pressure), which are both thermodynamically stable, solid-state phases of carbon. In our study, thermal annealing was conducted slightly above the atmosphere pressure, therefore the PDA films were converted toward the graphite structure. The graphitization process, including the degree of ordering and the crystalline size, progressed as the annealing temperature increased. As the temperature increased, the $G(r)$ peaks became higher and sharper, indicating the tendency of transforming to a graphite-like structure (Figure 2c). The local atomic arrangement in PDA and cPDA annealed at lower temperatures show ordering within a subnanometer scale, which results in a quick reduction of the profile intensities in long-range. Specifically, for the PDA and cPDA-600 samples, $G(r)$ flatten out beyond 0.6 nm, which corresponded to the dimension of the largest structural features in these materials. In

contrast, cPDA-800 and cPDA-900 showed peaks at larger r, implying the existence of larger ordered features. Therefore, one may conclude that heat treatment at higher temperatures (e.g., 800 °C) promote some growth of the ordered subnanometer structures.

The local atomic arrangement of cPDA is confirmed to be similar as graphite by the PDF fitting. An example of cPDA-900 is shown in Figure 2d. Slight intensity misfit may be due to residual elements like O and N, which tend to reduce the lattice parameters due to their smaller size than C. The calculated lattice parameter a is about 2.447(2) Å for the cPDA samples, which is slightly smaller than that of graphite, a = 2.464(2) Å.[15] In contrast, the atomic arrangement perpendicular to the layers may not be well ordered. The interlayer atomic correlation at r ≈ 3.36 Å, which is the spacing between layers in graphite, does not exhibit significant intensity in the PDF. The subnano-scaled particle size also limits the periodic extension along this direction. The inset of Figure 2d shows the average particle diameter as a function of the annealing temperatures. Although the average particle size monotonically increased from 0.69(4) nm in cPDA-600 to 1.54(7) nm in cPDA-900, the majority of the carbonized cPDA still could not form more than two graphite-like unit cells in a single particle.

To explore the graphite-like structures, we conducted a series of Raman spectroscopy experiments on the PDA and cPDA thin films. Raman spectra of all samples show the presence of two distinct bands: D band near 1360 cm^{-1} and G band near 1570 cm^{-1} (Figure 3a). As the heat treatment temperature increased, the position of the G band gradually shifted from 1573 to 1603 cm^{-1} (Figure 3b). The intensity ratio between the D and G bands, I_D/I_G, grows with the heat treatment temperature (Figure 3b). The simultaneous blue shift of the G-band and the growth of I_D/I_G ratio could be attributed to either (i) the amorphization of graphite, or (ii) the conversion from amorphous carbon (a-C) to nanocrystalline graphite.[13] We will show that for cPDA, the evidence supports the second hypothesis.

As illustrated by the solid arrows in Figures 3c, d, both the G-band shift and I_D/I_G ratio initially increase, as the graphite breaks into nanocrystalline graphites (NC graphite), and then decrease as the NC graphite becomes amorphous carbon (a-C). Further amorphization to tetragonal carbon (ta-C) will decrease I_D/I_G (Figure 3d) but increase the G-band shift (Figure 3c). This trend is reversible in the case of converting pure amorphous carbon to graphite. However, if impurity exists, the G band shift and the I_D/I_G ratio may follow different trajectories, as illustrated by the dashed arrows in Figures 3c, d.

As previously discussed, the TEM and diffraction results show PDA and cPDA films were mostly amorphous with some subnanometer features that were enlarged as the heat treatment temperature increased. Therefore, the shift of G-band toward higher wavenumbers and the increase of I_D/I_G (Figure 3b) are likely due to the heat-treatment induced structural conversion from a-C to NC graphite. Furthermore, since other elements are present, it is not surprising that the trends in Raman shift of G-band and I_D/I_G ratio (Figure 3b) deviated from the trajectory indicated by the solid line in Figures 3c, d.

Electrical conductivity and thermoelectric Seebeck coefficient were measured at ambient conditions (Figure S1). PDA and cPDA films heat-treated below 600 °C were electrically insulating and no Seebeck voltage could be measured. For samples heat-treated between 600 and 900 °C, a significant increase in electrical conductivity was observed with increasing

temperature of treatment (Figure 4a). Seebeck coefficients showed negative values (Figure 4a), indicating cPDA is an n-
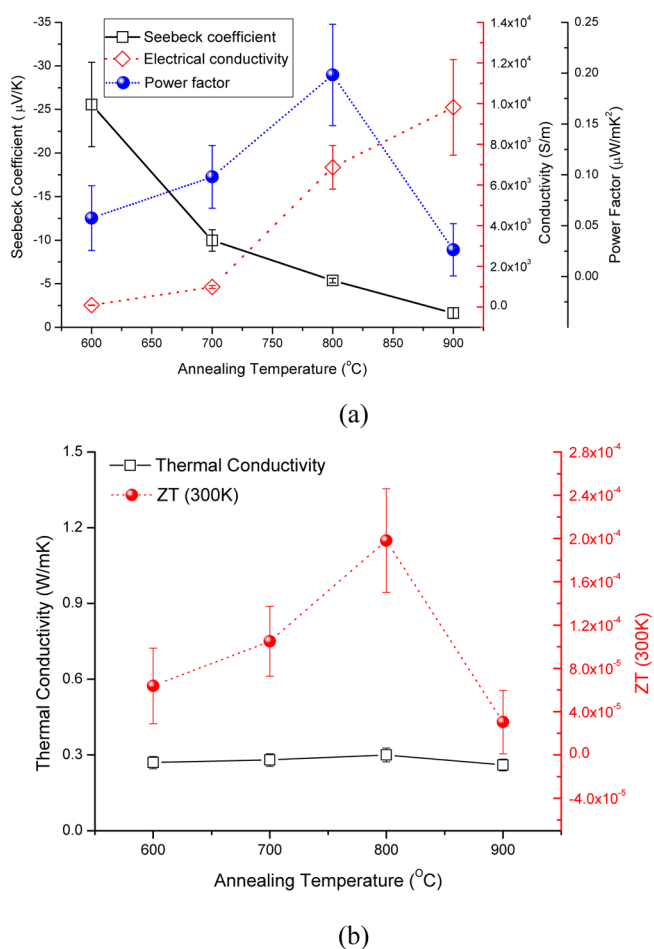

(a)

(b)

Figure 4. (a) Seebeck coefficient, electrical conductivity, and power factor respective to annealing temperature. (b) Thermal conductivity measured by TDTR and figure of merit respective to annealing temperature.

type semiconductor. The magnitude of the Seebeck coefficient decreased from around 25 μV/K for cPDA-600 to less than 5 μV/K for cPDA-900. Figure 4a also shows the trend of the power factor as a function of the heat treatment temperature, which has a peak value of 0.20 μW/(m K^2) for cPDA-800.

Recently, studies of thermoelectric properties of graphene have attracted much attention. Although pristine graphene is a gapless semiconductor, its electrical conductivity shows strong energy dependence near the charge neutrality point,[16] yielding finite Seebeck coefficients. Theoretical calculations indicated that the maximum Seebeck coefficient of pristine graphene is less than 100 μV/K at room temperature,[17] which was confirmed by several experiments.[18−20] Various strategies have been proposed to enhance the thermoelectric properties of graphene such as forming nanostructures and introducing defects.[21−24]

Besides graphene, thermoelectric properties of reduced graphene oxide (rGO) have also been studied. Xiao and co-workers[22] showed the Seebeck coefficient of rGO decreased from 17 to −7 μV/K when the temperature increased from 300 to 550 K, whereas the electrical conductivity increased from 2 × 10^3 to 9 × 10^3 S/m. Choi and co-workers[25] examined the

Seebeck coefficient and the electrical conductivity of rGO samples at room temperature. As the oxidation level increased, the Seebeck coefficient increased from 11 to 60 μV/K, whereas the electrical conductivity decreased from 880 to 0.14 S/m. The largest power factor obtained by Choi et al.[25] was 0.11 μW/(m K^2). Choi and coauthors[25] also mentioned that thermal conductivities of the rGO samples were as low as 0.3 W/(m K). However, the authors did not provide details on thermal conductivity measurements.[25]

In the current study, thermal conductivity was measured for PDA and cPDA thin films deposited on Si substrate using the time domain thermoreflectance (TDTR) method.[26−29] The thermal conductivity, shown on the left axis of Figure 4b, for all samples was around 0.3 W/(m K) with little variations. For TDTR on thin films ($\sim$30 nm), it is not possible to separately determine the contributions of the Al-cPDA thermal interface resistance ($R_{Al\text{-}cPDA}$) from the thermal resistance of the film itself ($R_{film} = t/\kappa_{film} = 30$ nm/0.3 W/(m K) $= 1 \times 10^{-7}$ (m^2 K)/W). Thus, we report the lower bound of the thermal conductivity, neglecting interfacial resistance. However, Schmidt[30] has previously measured the thermal interface conductance of Al on highly oriented pyrolytic graphite and found an interface conductance value of $\sim$50 MW/(m^2 K) near room temperature. Assuming similar values hold for cPDA, i.e., $R_{Al\text{-}cPDA} = 1/(50$ MW/(m^2 K)) $= 0.2 \times 10^{-7}$ (m^2 K)/W, the film would represent 80% of the total thermal resistance. Thereby, measured thermal conductivity values are similar to those reported by Choi et al. for rGO samples.[25] Because of the large aspect ratio between the laser spot size ($\sim$25 000 nm) and the film thickness ($\sim$30 nm), the measurements were essentially one-dimensional, having sensitivity only in the through-plane direction. Despite recent advances in measurement of in-plane thermal conductivity using TDTR,[28,29] the smallest achievable TDTR spot sizes and the lowest practical modulation frequencies are still not sufficient to directly measure the in-plane thermal conductivity for thin films with thermal conductivities as low as in the cPDA films.

It is important to note that the electrical conductivity and the Seebeck coefficient were measured in the direction parallel to the substrate. Because the XRD and TEM analyses did not show significant in-plane preferential crystallization/orientation, one may assume that there is no significant anisotropy in the transport properties. The dimensionless figure of merit (ZT) at room temperature ($T = 297$ K) can be calculated and shown in Figure 4b. In this study, the highest ZT of 2×10^{-4} was obtained from the cPDA films heat-treated at 800 °C, which is higher than that for rGO,[25] but is much lower than other state-of-the-art thermoelectric materials. Future studies should explore means to improve the electrical and thermoelectric properties, which may be obtained by optimizing the processing conditions and through elemental doping. Other properties, including mechanical properties, are also of interest.

In summary, this study revealed the amorphous nature of PDA and growth of nanostructural graphite during heat treatment. The thermal annealing method can yield large-scale cPDA thin films on many substrates. By controlling the annealing temperature, as demonstrated in this work, various electrical properties could be obtained, which may be utilized toward electronic applications.

■ ASSOCIATED CONTENT

ⓢ Supporting Information

The Supporting Information is available free of charge on the ACS Publications website at DOI: 10.1021/acsami.6b15601.

Experimental details, TGA, AFM and XRD results (PDF)

■ AUTHOR INFORMATION

Corresponding Author

*E-mail: renfei@temple.edu.

ORCID ⓘ

Haoqi Li: 0000-0002-9943-329X

Author Contributions

H.L prepared samples and conducted experiments including SEM, AFM, TEM, XRD, TGA, and electrical conductivity and Seebeck coefficient measurements. Y.V.A., L.F., and E.B. conducted the Raman spectroscopy measurements and data analyses. J.F. and R.K conducted the TDTR experiments and data analyses. Y.C. and K.A. performed the neutron experiments and data analyses. D.A.D. provided technical assistance in the measurements and discussion of the results. F.R. designed and guided the project. All authors have contributed to the manuscript revision.

Notes

The authors declare no competing financial interest.

■ REFERENCES

(1) Lee, H.; Dellatore, S. M.; Miller, W. M.; Messersmith, P. B. Mussel-Inspired Surface Chemistry for Multifunctional Coatings. *Science* **2007**, *318*, 426−430.

(2) Krogsgaard, M.; Nue, V.; Birkedal, H. Mussel-Inspired Materials: Self-Healing through Coordination Chemistry. *Chem. - Eur. J.* **2016**, *22*, 844−857.

(3) Meng, S.; Kaxiras, E. Theoretical Models of Eumelanin Protomolecules and Their Optical Properties. *Biophys. J.* **2008**, *94*, 2095−2105.

(4) Hong, S.; Na, Y. S.; Choi, S.; Song, I. T.; Kim, W. Y.; Lee, H. Non-Covalent Self-Assembly and Covalent Polymerization Co-Contribute to Polydopamine Formation. *Adv. Funct. Mater.* **2012**, *22*, 4711−4717.

(5) Liebscher, J.; Mrowczynski, R.; Scheidt, H. A.; Filip, C.; Hadade, N. D.; Turcu, R.; Bende, A.; Beck, S. Structure of Polydopamine: A Never-Ending Story? *Langmuir* **2013**, *29*, 10539−10548.

(6) Dreyer, D. R.; Miller, D. J.; Freeman, B. D.; Paul, D. R.; Bielawski, C. W. Elucidating the Structure of Poly(dopamine). *Langmuir* **2012**, *28*, 6428−6435.

(7) Li, R.; Parvez, K.; Hinkel, F.; Feng, X.; Muellen, K. va Bioinspired Wafer-Scale Production of Highly Stretchable Carbon Films for Transparent Conductive Electrodes. *Angew. Chem., Int. Ed.* **2013**, *52*, 5535−5538.

(8) Kong, J.; Yee, W. A.; Yang, L.; Wei, Y.; Phua, S. L.; Ong, H. G.; Ang, J. M.; Li, X.; Lu, X. Highly Electrically Conductive Layered Carbon Derived from Polydopamine and its Functions in SnO2-based Lithium Ion Battery Anodes. *Chem. Commun.* **2012**, *48*, 10316−10318.

(9) Ai, K.; Liu, Y.; Ruan, C.; Lu, L.; Lu, G. Sp2 C-Dominant N-Doped Carbon Sub-micrometer Spheres with a Tunable Size: A Versatile Platform for Highly Efficient Oxygen-Reduction Catalysts. *Adv. Mater.* **2013**, *25*, 998−1003.

(10) Yu, X.; Fan, H.; Liu, Y.; Shi, Z.; Jin, Z. Characterization of Carbonized Polydopamine Nanoparticles Suggests Ordered Supramolecular Structure of Polydopamine. *Langmuir* **2014**, *30*, 5497−5505.

(11) Ryu, S.; Chou, J. B.; Lee, K.; Lee, D.; Hong, S. H.; Zhao, R.; Lee, H.; Kim, S. Direct Insulation-to-Conduction Transformation of Adhesive Catecholamine for Simultaneous Increases of Electrical Conductivity and Mechanical Strength of CNT Fibers. *Adv. Mater.* **2015**, *27*, 3250−3255.

(12) Ryu, J.; Ku, S. H.; Lee, M.; Park, C. B. Bone-Like Peptide/hydroxyapatite Nanocomposites Assembled with Multi-Level Hierarchical Structures. *Soft Matter* **2011**, *7*, 7201−7206.

(13) Ferrari, A. C.; Robertson, J. Raman Spectroscopy of Amorphous, Nanostructured, Diamond-Like Carbon, and Nanodiamond. *Philos. Trans. R. Soc., A* **2004**, *362*, 2477−2512.

(14) Ferrari, A. C. Raman Spectroscopy of Graphene and Graphite: Disorder, Electron-Phonon Coupling, Doping and Nonadiabatic Effects. *Solid State Commun.* **2007**, *143*, 47−57.

(15) Trucano, P.; Chen, R. Structure of Graphite by Neutron-Diffraction. *Nature* **1975**, *258*, 136−137.

(16) Novoselov, K.; Geim, A.; Morozov, S.; Jiang, D.; Katsnelson, M.; Grigorieva, I.; Dubonos, S.; Firsov, A. Two-Dimensional Gas of Massless Dirac Fermions in Graphene. *Nature* **2005**, *438*, 197−200.

(17) Ouyang, Y.; Guo, J. A Theoretical Study on Thermoelectric Properties of Graphene Nanoribbons. *Appl. Phys. Lett.* **2009**, *94*, 263107.

(18) Zuev, Y. M.; Chang, W.; Kim, P. Thermoelectric and Magnetothermoelectric Transport Measurements of Graphene. *Phys. Rev. Lett.* **2009**, *102*, 096807.

(19) Wei, P.; Bao, W.; Pu, Y.; Lau, C. N.; Shi, J. Anomalous Thermoelectric Transport of Dirac Particles in Graphene. *Phys. Rev. Lett.* **2009**, *102*, 166808.

(20) Checkelsky, J. G.; Ong, N. P. Thermopower and Nernst Effect in Graphene in a Magnetic Field. *Phys. Rev. B: Condens. Matter Mater. Phys.* **2009**, *80*, 081413.

(21) Dragoman, D.; Dragoman, M. Giant Thermoelectric Effect in Graphene. *Appl. Phys. Lett.* **2007**, *91*, 203116.

(22) Xiao, N.; Dong, X.; Song, L.; Liu, D.; Tay, Y.; Wu, S.; Li, L.; Zhao, Y.; Yu, T.; Zhang, H.; Huang, W.; Hng, H. H.; Ajayan, P. M.; Yan, Q. Enhanced Thermopower of Graphene Films with Oxygen Plasma Treatment. *ACS Nano* **2011**, *5*, 2749−2755.

(23) Xu, Y.; Li, Z.; Duan, W. Thermal and Thermoelectric Properties of Graphene. *Small* **2014**, *10*, 2182−2199.

(24) Dollfus, P.; Nguyen, V. H.; Saint-Martin, J. Thermoelectric Effects in Graphene Nanostructures. *J. Phys.: Condens. Matter* **2015**, *27*, 133204.

(25) Choi, J.; Tu, N. D. K.; Lee, S.; Lee, H.; Kim, J. S.; Kim, H. Controlled Oxidation Level of Reduced Graphene Oxides and its Effect on Thermoelectric Properties. *Macromol. Res.* **2014**, *22*, 1104−1108.

(26) Cahill, D. Analysis of Heat Flow in Layered Structures for Time-Domain Thermoreflectance. *Rev. Sci. Instrum.* **2004**, *75*, 5119−5122.

(27) Kang, K.; Koh, Y. K.; Chiritescu, C.; Zheng, X.; Cahill, D. G. Two-Tint Pump-Probe Measurements Using a Femtosecond Laser Oscillator and Sharp-Edged Optical Filters. *Rev. Sci. Instrum.* **2008**, *79*, 114901.

(28) Feser, J. P.; Cahill, D. G. Probing Anisotropic Heat Transport Using Time-Domain Thermoreflectance with Offset Laser Spots. *Rev. Sci. Instrum.* **2012**, *83*, 104901.

(29) Feser, J. P.; Liu, J.; Cahill, D. G. Pump-Probe Measurements of the Thermal Conductivity Tensor for Materials Lacking in-Plane Symmetry. *Rev. Sci. Instrum.* **2014**, *85*, 104903.

(30) Schmidt, A. J.; Collins, K. C.; Minnich, A. J.; Chen, G. Thermal Conductance and Phonon Transmissivity of Metal-Graphite Interfaces. *J. Appl. Phys.* **2010**, *107*, 104907.